PHYSICAL REVIEW B
CONDENSED MATTER

THIRD SERIES, VOLUME 44, NUMBER 18 1 NOVEMBER 1991-II

Kinetics of short-range and long-range $B2$ ordering in FeCo

B. Fultz
California Institute of Technology, 138-78, Pasadena, California 91125
(Received 7 June 1991)

Short-range and long-range-order parameters were measured by Mössbauer spectrometry and x-ray diffractometry during the disorder $\rightarrow B2$ order transformation in equiatomic FeCo. The change from a homogeneous mode of ordering at high temperatures to a heterogeneous mode of ordering at low temperatures was confirmed. By comparing parametric plots of the ^{57}Fe hyperfine magnetic field versus long-range-order parameter for ordering in these two modes, an early independent relaxation of the short-range order was found in the kinetic path for homogeneous ordering. This relaxation was in reasonable agreement with estimates based on statistical kinetic theory.

I. INTRODUCTION

Ordering in equiatomic FeCo has been studied by many previous investigators.[1-25] The kinetics of the disorder$\rightarrow$order transformation are usually studied by measuring the time dependence of the long-range-order (LRO) parameter[6,9,12,13,15] or a short-range-order (SRO) parameter.[24] The present study takes the different approach of simultaneously monitoring the SRO and LRO. Rather than emphasizing the temporal evolution of these order parameters, the present work emphasizes the "kinetic path" of the material through different combinations of SRO and LRO; i.e., how kinetics affects the nonequilibrium structural states that evolve in the material. Because interpretations of kinetic paths in terms of the atomic jump mechanism do not require knowledge of the actual vacancy concentration, kinetic path experiments are more easily interpreted than temporal evolution experiments. As shown recently by our group,[25-30] initially disordered alloys may take a wide range of kinetic paths *en route* to their final state of thermodynamic equilibrium.

It is a challenge for statistical kinetic theory of ordering by vacancies to manipulate more than one order parameter, but such sophistication is required for the proper understanding of disorder$\rightarrow$order transformations. Even the apparently simple problem of the evolution of $B2$ order in a binary alloy in the pair approximation illustrates how temperature can be used to control the kinetic paths through the space spanned by the pair variable, $p_{AA}^{\alpha\beta}$, and the point variable, p_A^{α}.[27] (For a binary alloy of A and B atoms, the point variable, p_A^{α}, is the probability that a site on the A-rich, α sublattice of the $B2$ structure is occupied by an A atom, while the pair variable, $p_{AA}^{\alpha\beta}$, is the probability that a specific first neighbor bond between the α sublattice and β sublattice will be between two A atoms.) Some previous theoretical results for the evolution of the SRO pair variable, $p_{AA}^{\alpha\beta}$, and the LRO point variable, p_A^{α}, are compiled in Fig. 1. The kinetic path in the pair (Bethe, or quasichemical) approximation was obtained by the integration of the kinetic master equation as described previously.[27] The kinetic path in the point (random mixing or mean-field) approximation is a simple parabola because the point and pair variables are not independent in this approximation. Also presented in Fig. 1 are results from Monte Carlo simulations with an algorithm used previously[31-33] and described more fully in Sec. III. C.

The salient change in kinetic path when going beyond the point approximation is in the early stage of ordering, where a quick relaxation of the SRO (pair variable) occurs without the relaxation of the LRO (point variable). This was reported previously by Gschwend, Sato, and Kikuchi[34-36] and Fultz.[27] Monte Carlo simulations also predict this same early SRO relaxation. In a disordered alloy there is a wide distribution of local atom configurations, and the early, independent relaxation of SRO occurs as atoms in less energetically favorable environments jump with a higher probability into adjacent vacancies. Statistical kinetic theories show that order does not evolve fully with this quick relaxation of SRO; the evolution of LRO is necessary to sustain a substantial range of energies in the different local environments. As LRO evolves, each atom species has an increasing preference for one sublattice, and with this growing differentiation of site energies, the SRO and LRO evolve together towards thermodynamic equilibrium.

It is intuitive that, in the early stages of ordering the

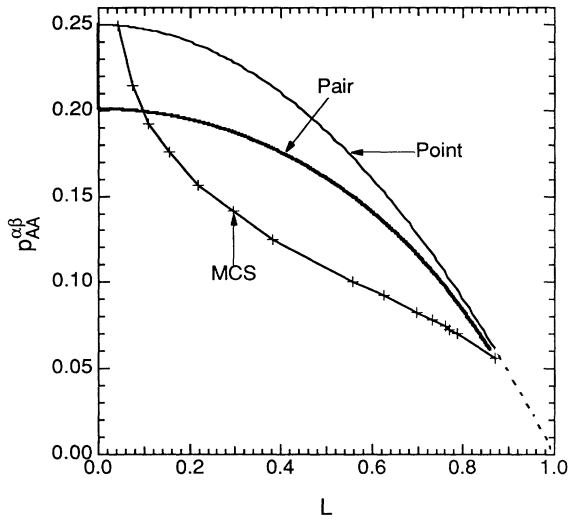

FIG. 1. Calculated kinetic paths through the SRO (pair variable, $p_{AA}^{\alpha\beta}$) and the LRO (L) for analytical point and pair approximations (Refs. 27 and 34–36), and Monte Carlo simulations. The alloy was equiatomic bcc with two sublattices, and all methods used atomic pair potentials $V_{AA}=V_{BB}=0.41kT$, all other $V=0$, and equal activation barrier heights for A and B atoms. For a critical temperature of 730 °C and a critical potential of 0.3147, these parameters correspond to annealing at 500 °C. The initial state of disorder is in the upper left corner, and the kinetic path proceeds to an equilibrium state in the lower right. For the Monte Carlo simulation, the line connects the data points in their temporal sequence.

SRO should relax more quickly than the LRO, but Fig. 1 shows that statistical kinetic theory makes a quantitative prediction for the amount of this relaxation. This prediction cannot be obtained directly from thermodynamics or by statistical kinetic theory in approximations lower than the pair. I undertook the present investigation to find and to measure this early, independent relaxation of SRO in the disorder→order transformation in rapidly quenched FeCo. X-ray diffractometry was used to measure LRO in the conventional way by comparing the intensities of $B2$ superlattice diffractions to the intensities of the fundamental bcc diffractions. Problems with the small difference in x-ray scattering factors of Fe and Co atoms were overcome by using Co $K\alpha$ radiation to suppress the scattering factor of the Fe atoms, and by using a large-angle position-sensitive detector for simultaneous data collection at all 2θ angles. Even with these experimental capabilities, it was not practical to measure the SRO by x-ray diffuse scattering. Instead, Mössbauer spectrometry was used to measure the evolution of SRO. Unlike x-ray diffractometry, which makes direct measurements of correlations between atom positions, Mössbauer spectrometry is sensitive to local magnetic disturbances in the material through the ^{57}Fe hyperfine magnetic field (HMF), and is a less direct measure of SRO. It is known, however, how variations in local atomic configurations affect the HMF in Fe-Co alloys,[23,24,37–39] so models of the SRO can be tested against observed HMF distributions. I am, nevertheless, cautious about using the systematics of HMF responses to local magnetic moments for obtaining direct structural information from Mössbauer spectra. It is better to use Mössbauer spectrometry to obtain trends in the SRO evolution, and it is better still to use Mössbauer spectrometry for a comparative study of different kinetic paths. Fortunately, because of a change in the mode of ordering from homogeneous to heterogeneous, such a comparative study was possible in equiatomic FeCo.

II. EXPERIMENT

The preparation of the Fe–50-at. % Co. ingot, including measurements of composition and purity, was described previously.[24,29] Small pieces of the ingot were levitation melted and then rapidly quenched by the piston-anvil technique. Annealings were performed by sealing the splat foils in evacuated borosilicate glass ampules, but for annealings of less than a minute, the splat foils were sandwiched briefly between a pair of aluminum blocks that had previously equilibrated in the furnace. The heating rate of a thermocouple subjected to this latter procedure was more than 300 °C/s. Surface oxides were found in the diffraction profiles of many of the materials annealed in this way, but the oxides were eliminated by chemical polishing, and each splat foil was subjected to only one rapid annealing.

Mössbauer spectra at 25 °C were obtained in transmission geometry with a conventional constant acceleration spectrometer. A radiation source of 20 mCi ^{57}Co in a Rh matrix was used for all measurements. The spectrometer velocity calibration was checked after every run by obtaining a spectrum from a pure Fe foil. The specimens used in this work were about 15 μm thick, and no thickness distortion corrections were employed. X-ray diffraction was performed with a Debye-Scherrer diffractometer using an Inel CPS-120 position-sensitive detector that spanned an arc of 127° in 2θ angle. The incident radiation was Co $K\alpha_{1,2}$ monochromated with graphite. To obtain good statistics for the (100), (111), and (210) $B2$ superlattice diffractions, the integrated counts in the (110) and (200) fundamental bcc peaks ranged from $(0.2–2.0)\times10^8$. Around the (110) diffraction, the peak-to-background ratio was about 300.

III. RESULTS OF EXPERIMENTS AND MONTE CARLO SIMULATIONS

A. X-ray diffraction

The integrated intensities of the x-ray-diffraction peaks from the fixed position-sensitive detector and flat specimens were corrected by the polarization and geometry factor:

$$I_{PG}(\theta)=mF^*(\Delta k)F(\Delta k)\frac{1+\cos^2\theta}{\sin 2\theta}\frac{\sin\zeta}{\sin\phi+\sin\zeta}D(\Delta k)\ , \tag{1}$$

where m is the multiplicity, $F(\Delta k)$ is the atomic scattering factor, ϕ is the angle of the incident beam with

respect to the plane of the flat sample (generally 20°), and ζ is the angle of the diffracted beam. (Note that $2\theta=\phi+\zeta$.) Assuming a Debye temperature of 440 K, the Debye-Waller factor, $D(\Delta k)$, ranged from about 0.98 for the (100) diffraction to 0.86 for the (220) diffraction. The relative ratios of the fundamental peaks remained approximately constant for all samples, so corrected, integrated intensities of the (110), (200), and (211) fundamental bcc peaks were summed, as were the total intensities of the (100) (111), and (210) $B2$ superlattice diffractions. The LRO parameter, L, was then proportional to the square root of the ratio of the summed superlattice intensity to the summed fundamental intensity. It is difficult to obtain an absolute calibration for the LRO parameter because the scattering factor difference, $f_{\mathrm{Co}}-f_{\mathrm{Fe}}$, is very sensitive to the dispersion correction for f_{Fe} under Co $K\alpha$ radiation. Conversely, by using the equilibrium LRO calculated with the Monte Carlo simulation (about 0.87 at 500 °C from Fig. 1), we estimated the scattering factor difference, $f_{\mathrm{Co}}-f_{\mathrm{Fe}}\approx 3.9$. Using this calibration from the end state of the Monte Carlo simulation and the steady state of the annealed samples, the evolution of the LRO parameter as a function of time at different temperatures is presented in Fig. 2.

The $B2$ superlattice diffractions observed after short annealings at 520 and 570 °C were broadened significantly with respect to the fundamental diffractions as reported by Buckley.[12] This broadening is certainly caused by the small characteristic size of the ordered domains, since the sharp fundamental diffractions will sense approximately the same strain distributions. This was confirmed when the superlattice diffractions were fit to the convolution of a Lorentzian and Gaussian function plus a linear background. The widths of the Gaussian and Lorentzian components of the diffraction peaks, $w_G(\theta)$ and $w_L(\theta)$, were converted to Δk $[w(\Delta k)=w(\theta)4\pi\cos\theta\lambda^{-1}]$, and plotted against Δk $(\Delta k=4\pi\sin\theta\lambda^{-1})$. The Lorentzian component had little dependence on Δk, and the slope of the Gaussian component was a mean squared strain of 0.0036. From the average of the half-widths of the Lorentzian components of the (100) (111), and (210) diffractions, the characteristic domain size was obtained; the inverse of this average half-width is the length $\langle l\rangle$, of the exponential domain size distribution corresponding to the Lorentzian line shape[40]

$$P(l)=\frac{1}{\langle l\rangle}\exp\left[-\frac{l}{\langle l\rangle}\right]. \tag{2}$$

The growth of the domain size $\langle l\rangle$ at different temperatures is presented in Fig. 3.

B. Mössbauer spectrometry

The ^{57}Fe hyperfine magnetic field distributions were obtained from the Mössbauer spectra by a curve-fitting procedure similar to that used previously.[24] A Gaussian distribution was used to express the HMF distribution, $P(H)$:

$$P(H)=A\exp\left[-\left[\frac{H-\langle H\rangle}{\sigma}\right]^2\right], \tag{3}$$

where A is a normalization constant, $\langle H\rangle$ is the mean HMF, and σ is the standard deviation. This HMF distribution was converted to a Gaussian velocity distribution for each absorption peak, and was convolved with a Lorentzian function having a width characteristic of the absorption peaks in a pure Fe spectrum. A linear background was then added to the result, and the total peak plus background function was least-squares fitted to the peaks in the spectrum. In the fitting routine, the parameters A, $\langle H\rangle$, σ, and the background were all varied in-

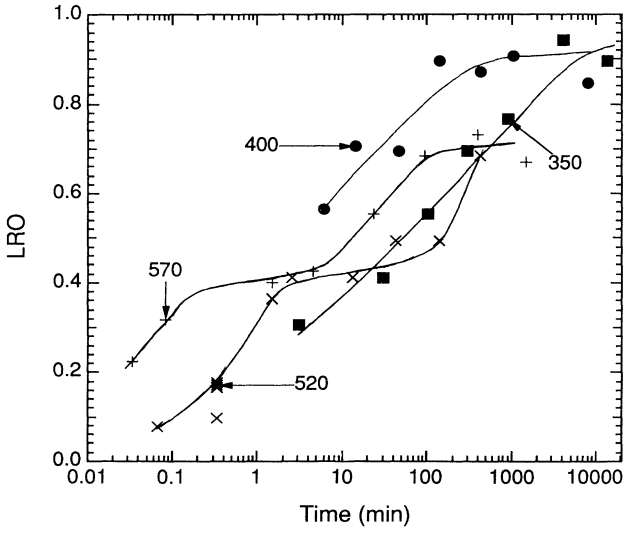

FIG. 2. Evolution of LRO in piston-anvil quenched FeCo after annealing at temperatures of 350, 400, and 570 °C for various times. Lines are drawn to guide the eye.

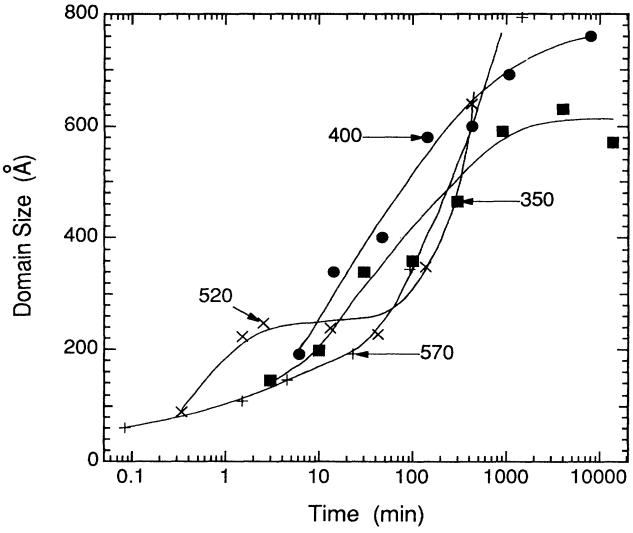

FIG. 3. Growth of the characteristic length of the ordered regions in piston-anvil quenched FeCo after annealing at temperatures of 350, 400, 520 and 570 °C for various times. Lines are drawn to guide the eye.

dependently. To avoid interference with the tails of peaks 2 and 5, these two peaks were fit first, and then stripped from the spectrum. The central velocities of peaks 1 and 6 were then used to obtain the average hyperfine magnetic field, $\langle H \rangle$, which changed during annealing as shown in Fig. 4.

C. Monte Carlo simulations

In previous work we developed Monte Carlo algorithms to simulate diffusion and ordering with an activated state rate theory for vacancy jumps.[31–33] The assumptions about how the local chemical environment affects the probability of a vacancy jump are the same as in the analytical theories,[27–29,34–36] but the Monte Carlo simulations are exact for a periodic lattice of finite size. The Monte Carlo simulations are particularly useful because x-ray diffractometry and Mössbauer spectrometry "experiments" can be performed on the simulated alloys. The x-ray-diffraction pattern is easily simulated within kinematical theory by taking the diffracted wave $\Psi(\Delta k)$ as the three-dimensional Fourier transform of the alloy, and then calculating $\Psi^*\Psi$:

$$\Psi^*(\Delta k)\Psi(\Delta k)=\left|\sum_{\text{all sites}} f(\mathbf{r})\exp(-i\Delta\mathbf{k}\cdot\mathbf{r})\right|^2 . \quad (4)$$

For simplicity, the scattering factors of the A atoms were set to unity, and the scattering factors of the B atoms were set to zero, so the diffracted wave was obtained as the sum of all $\exp(-i\Delta\mathbf{k}\cdot\mathbf{r})$ at the positions $\mathbf{r}$ of the A atoms. The intensities of the diffraction peaks were obtained by integrating $\Psi^*\Psi$ in a cubical volume around the center of the diffraction peak with a width in $\Delta\mathbf{k}$ that corresponded to our experimental capability. A width in $\Delta\mathbf{k}$ of $0.10\times 2\pi/a$ was used, where a is the edge length of the cubic bcc unit cell. Similar results were obtained when the width in $\Delta\mathbf{k}$ was as large as $0.30\times 2\pi/a$, but when the width in $\Delta\mathbf{k}$ became too large, the integration included the diffuse scattering, and there was little structure to the kinetic path of SRO versus LRO.

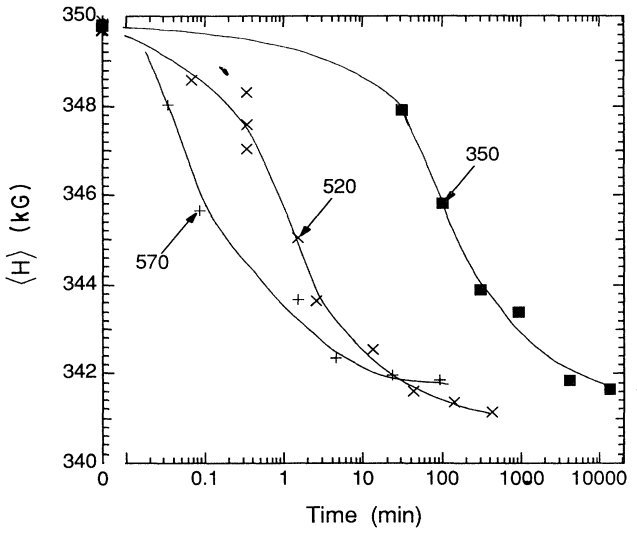

FIG. 4. Change in the average ^{57}Fe HMF in piston-anvil quenched FeCo after annealing at temperatures of 350, 520, and 570 °C for various times. Lines are drawn to guide the eye.

Simulated Mössbauer spectra from FeCo alloys were obtained from the alloys of the Monte Carlo simulations. The model of ^{57}Fe HMF responses to the configurations of local magnetic moments[37,39] is too involved to present here, but suffice to say that the 4s conduction electron polarization seen at a ^{57}Fe nucleus owing to the surrounding atoms is included, as is the core s-electron polarization due to the effects on the ^{57}Fe magnetic moment owing to the surrounding Co neighbors. The present work employed the same mechanisms used previously for the ^{57}Fe HMF response to the Co and Fe magnetic moments, and the parameters for these responses and the values of the magnetic moments were the same as used previously.[24,38] Again, it was necessary to linearly scale the magnitude of the changes in HMF during ordering to correspond to the actual experimental results.

IV. DISCUSSION

A. Heterogeneous mode of ordering

The specific heat of the order-disorder transformation in FeCo has a λ-type temperature dependence with little hysteresis,[1,3,4,9,11] and the equilibrium value of the LRO parameter increases continuously below the critical temperature of 730 °C.[5,9] This is strong evidence that the order-disorder transformation in FeCo is of second order in free energy, as permitted by the Landau-Lifshitz criterion. In general, we expect that lower temperatures will increasingly favor second-order phase transformations as the thermodynamic driving forces become greater.

It was reported by Buckley[12] that ordering in quenched FeCo changes from a homogeneous mode at high temperatures to a heterogeneous mode at low temperatures. At low temperatures, the ordered phase was found to nucleate at grain boundaries and then grow into the disordered phase in a first-order phase transformation. This change in mode to heterogeneous ordering at low temperatures is contrary to thermodynamic predictions and must be a kinetic phenomenon. It could be related to vacancy availability; vacancies may be supplied by grain boundaries, and at low temperatures they may remain trapped near the propagating order-disorder interface.[32]

Buckley's picture of the mode change is consistent with the present results. The rate of long-range ordering (Fig. 2) increases from 350 to 400 °C, and again between 520 and 570 °C, but ordering at 520 °C is much slower than at 400 °C. The size of the ordered domains also increases most rapidly at the lowest temperatures (Fig. 3), consistent with a strong driving force for propagating well-ordered domains into the disordered solid solution. Once the ordered regions have grown over the entire grain, the microstructural evolution slows considerably because coarsening of the ordered domains would proceed in a manner similar to the domain growth at higher temperatures. That a different microstructure evolves in these two temperature ranges is also shown by the parametric plot of Fig. 5. With the nucleation and growth of an or-

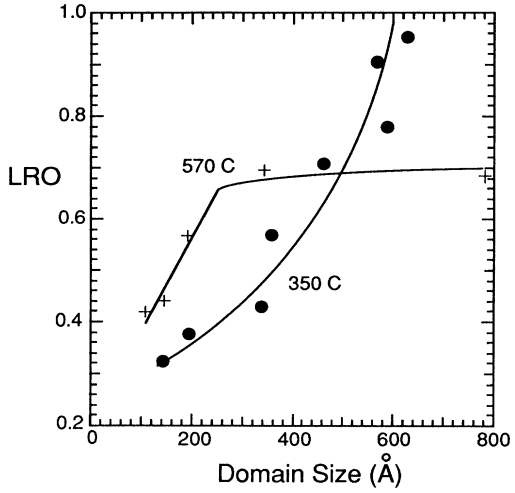

FIG. 5. Parametric plot of LRO vs characteristic size of ordered domains for alloys annealed at 350 and 570 °C for various times. Lines are drawn to guide the eye.

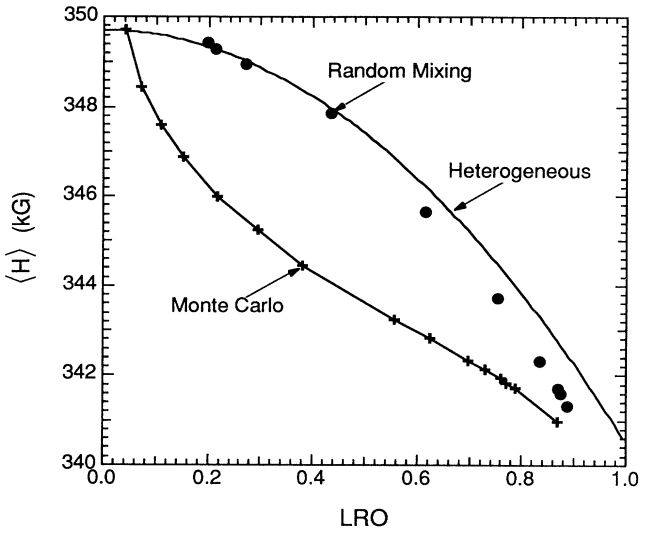

FIG. 6. Simulated and calculated kinetic paths of ^{57}Fe HMF vs x-ray LRO parameter for disorder→order transformation in FeCo. The three data sets are: (i) Monte Carlo simulations of ordering with vacancies (same simulations used for the data of Fig. 1), line is drawn to guide the eye; (ii) the same Monte Carlo simulations, but with the atomic species randomly mixed on the two $B2$ sublattices during calculations of $\langle H \rangle$ and L; (iii) heterogeneous ordering, line is calculated with Eqs. (5) and (6).

dered region, the average LRO will be smaller for a given size of ordered domain than if a moderate degree of order evolved homogeneously throughout the material.

In the nucleation and growth mode of ordering, the x-ray diffractometry profiles and the Mössbauer spectra comprise a sum of two components, one from the disordered region and one from the ordered region. The fractions of these components are equal to the fractions of the disordered and ordered regions. In the nucleation and growth mode, the SRO and LRO parameters are not independent of each other because they are both dependent on the fraction of ordered region. The SRO therefore cannot grow without growth of the LRO. The average HMF obtained from a Mössbauer spectrum of an alloy partially ordered by the nucleation and growth mechanism is

$$\langle H \rangle = H_{\text{ord}} f_{\text{ord}} + H_{\text{dis}}(1 - f_{\text{ord}}) , \tag{5}$$

where the fraction of the ordered phase is f_{ord}, the ordered phase has a HMF $H_{\text{ord}} \cong 340.5$ kG, and the disordered phase has a HMF $H_{\text{dis}} = 349.7$ kG (both at 23 °C). For the nucleation an growth mode of ordering, the apparent LRO parameter L is

$$L = L_{\text{ord}} (f_{\text{ord}})^{1/2} . \tag{6}$$

From Eqs. (5) and (6) we see that a parametric plot of $\langle H \rangle$ versus L will be a parabola reminiscent of the point approximation in Fig. 1. On the other hand, for the homogeneous mode of ordering, both the pair approximation and the Monte Carlo simulations should predict a more rapid drop in $\langle H \rangle$ than in L during the early stages of ordering. The shape of this drop must be calculated from a detailed analysis of the HMF, and the results of this analysis are presented in the next section.

B. Kinetic path of homogeneous mode of ordering

Figure 6 presents the results of simulated experimental kinetic paths of $\langle H \rangle$ versus L, which correspond to SRO and LRO. One set of alloys was obtained by a Monte Carlo simulation of ordering with a vacancy mechanism, and from each state of the alloy, the Mössbauer and x-ray diffractometry data were simulated as sketched in Sec. III C. The second data set in Fig. 6 was obtained by a different sort of Monte Carlo simulation in which the alloy was decomposed into the two simple-cubic sublattices of the $B2$ structure, and the A and B atoms were arranged randomly on these two sublattices. The kinetic path through these single-domain alloys corresponds, of course, to that of the point (random mixing) approximation. The third kinetic path in Fig. 6 was calculated by assuming a heterogeneous mode of ordering where a region of equilibrium order grows into the region of disorder. This is just the parabolic relationship described by Eqs. (5) and (6). Figure 7 presents our experimental kinetic paths of $\langle H \rangle$ versus L. The excellent agreement between the kinetic paths at 350 and 400 °C in Fig. 7 and the heterogeneous curve in Fig. 6 is further evidence that $B2$ ordering in FeCo evolves heterogeneously at low temperatures.

More significant from the point of view of statistical kinetic theory is the agreement between the experimental kinetic paths at 520 and 570 °C in Fig. 7 and the simulated kinetic path for homogeneous ordering in Fig. 6. As in Fig. 1, the kinetic path begins in the upper left of the figure, and the first four data points (crosses) in Fig. 1 are those of the SRO relaxation; the same four states of the same simulated alloy were used to obtain the first four data points in Fig. 6. In the early, independent relaxation of SRO, $\langle H \rangle$ decreases relatively rapidly with respect to

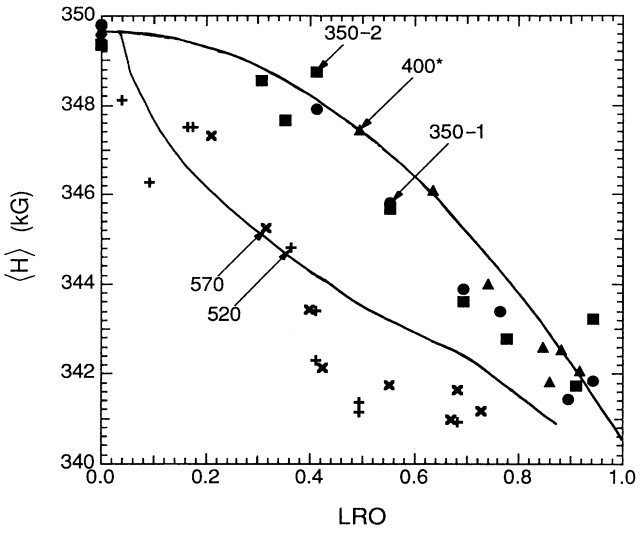

FIG. 7. Experimental kinetic paths of $\langle H \rangle$ vs L for piston-anvil quenched FeCo annealed at 350, 400, 520, and 570 °C for various times. Data set 350-1 was obtained in the present work, data set 350-2 was obtained previously (Ref. 24). Data set 400* was obtained by scaling previous data at 77 K (Ref. 24) to fit an 8 kG range in $\langle H \rangle$ (this should slightly underestimate the concave downward curvature). Lines are those of Fig. 6.

L, as expected since the HMF is sensitive to atomic arrangements within a few Å around the ^{57}Fe atom.[24] The strong difference in the initial slopes of the two kinetic paths in Fig. 7 reflects the early, independent relaxation of SRO, and the good agreement between the kinetic paths of Figs. 6 and 7 confirms approximately the magnitude of this relaxation predicted by the Monte Carlo simulations. (Variations in the temperature for the Monte Carlo simulations caused modest changes in the shape of the simulated experimental kinetic path.) Since the pair approximation and the Monte Carlo simulations showed qualitatively similar early, independent relaxations of the SRO (Fig. 1), there is also modest agreement between experiment and statistical kinetic theory in the pair approximation.

In spite of the good agreement between the calculated and measured kinetic paths of Figs. 6 and 7, it is reasonable to question whether the systematics of the HMF distribution are sufficiently well understood to provide such a good agreement between each calculated and measured kinetic path. (Conversely, if we accept the predictions of statistical kinetic theory, the good agreement between the individual curves provides support for the systematics of the ^{57}Fe HMF distribution in FeCo.) More reliable than the predictions of absolute kinetic paths in $\langle H \rangle$ versus L are the predicted differences in $\langle H \rangle$ versus L for the different modes of ordering. Clearly these differences are predicted well. Finally, it is interesting that the simulated experiment of a random-mixing kinetic path agrees so well with the simulated kinetic path of heterogeneous ordering. This agreement is expected for a kinetic path of a true SRO parameter like $p_{AA}^{\alpha\beta}$ versus L, but it is not obviously true for $\langle H \rangle$ versus L, and the simulations were used to reveal this trend. The average ^{57}Fe HMF, $\langle H \rangle$, therefore seems a good parametrization of SRO in FeCo. This is not unexpected since the characteristic length of the HMF sensitivity to local atomic arrangements is about 4 Å, and this sensitivity extends to only 9 Å.[24,39]

V. CONCLUSIONS

Two kinetic phenomena, independent of thermodynamic predictions, were observed in the ordering of rapidly quenched, equiatomic FeCo: (1) the present work corroborates the report by Buckley[12] that the mode of ordering undergoes a change from homogeneous at temperatures above 500 °C to heterogeneous at temperatures of 400 °C and below. (2) Statistical kinetic theory in the pair approximation and Monte Carlo simulations predict that $B2$ order will initially evolve from a disordered alloy with an early, independent relaxation of the SRO (without growth of the LRO). This behavior was confirmed qualitatively for the homogeneous ordering of FeCo above 500 °C. The experimentally measured kinetic paths through $\langle H \rangle$ and L (experimental SRO and LRO parameters) were in reasonable agreement with the calculated paths.

ACKNOWLEDGMENTS

I am pleased to acknowledge the help of L. Anthony with software development, D. H. Pearson with the ultrarapid quenching, and Z-Q. Gao with the x-ray diffractometry. This work was supported by the U. S. Dept. of Energy under contract No. DE-FG03-86ER45270.

[1]W. C. Ellis and E. S. Greiner, Trans. ASM **29** 415 (1941).
[2]C. G. Shull and S. Siegel, Phys. Rev. **75**, 1008 (1949).
[3]D. L. Martin and A. H. Geisler, Trans. ASM **44**, 461 (1952).
[4]A. J. Griest, J. F. Libsch, and G. P. Conard, Acta Metall. **3**, 509 (1955).
[5]N. S. Stoloff and R. G. Davies, Acta Metall. **12**, 473 (1964).
[6]A. T. English, Trans. AIME **236**, 14 (1966).
[7]B. deMayo, D. W. Forester, and S. Spooner, J. Appl. Phys. **41**, 1319 (1970).
[8]J. F. Dinhut, J. P. Eymery, and P. Moine, Phys. Status Solidi A **12**, 153 (1972).
[9]D. W. Clegg and R. A. Buckley, Metal Sci. **7**, 48 (1973).
[10]J. P. Eymery, P. Grosbras, and P. Moine, Phys. Status Solidi **21**, 517 (1974).
[11]J. Orehotsky and K. Schröder, J. Phys. F **4**, 196 (1974).
[12]R. A. Buckley, Metal. Sci. **9**, 243 (1975).
[13]Ye. I. Mat'tsev, V. I. Goman'kov, I. M. Puzey, V. A. Makarov, and Ye. V. Kozis, Fiz. Metal. Metalloved. **39**, 543 (1975).
[14]M. S. Seehra and P. Silinsky, Phys. Rev. B **13**, 5183 (1976).

[15]A. W. Smith and R. D. Rawlings, Phys. Status Solidi A **34**, 117 (1976).
[16]L. A. Alekseyev, D. M. Dzhavadov, Yu. D. Tyapkin, and R. B. Levi, Fiz. Metal. Metalloved. **43**, 1235 (1977).
[17]G. N. Belozerskiy, V. V. Dudoladov, and M. I. Kazakov, Fiz. Metal. Metalloved. **44**, 553 (1977).
[18]P. A. Montano and M. S. Seehra, Phys. Rev. B **5**, 2437 (1977).
[19]B. deMayo, Phys. Rev. B **24**, 6503 (1981).
[20]J. E. Frackowiak, Phys. Status Solidi A **87**, 109 (1985).
[21]B. Fultz, Hyperfine Interact. **41**, 607 (1988).
[22]R. J. Hawkins and J. M. Sanchez, J. Phys. F **18**, 767 (1988).
[23]B. Fultz and H. H. Hamdeh, Hyperfine Interact. **45**, 55 (1989).
[24]B. Fultz and H. H. Hamdeh, Philos. Mag. B **60**, 601 (1989).
[25]B. Fultz and H. H. Hamdeh, and D. H. Pearson, Acta Metall. **37**, 2841 (1989).
[26]B. Fultz, Acta Metall. **37**, 823 (1989).
[27]B. Fultz, J. Mater. Res. **5**, 1419 (1990).
[28]B. Fultz, J. Less-Common Met. **168**, 145 (1991).
[29]L. Anthony and B. Fultz, J. Mater. Res. **4**, 1132 (1989).
[30]L. Anthony and B. Fultz, J. Mater. Res. **4**, 1140 (1989).
[31]B. Fultz, J. Chem. Phys. **87**, 1604 (1987).
[32]B. Fultz, H. Chem. Phys. **88**, 3227 (1988).
[33]B. Fultz and L. Anthony, Philos. Mag. Lett. **59**, 237 (1989).
[34]H. Sato and R. Kikuchi, Acta Metall. **24**, 797 (1976).
[35]H. Sato, K. Gschwend, and R. Kikuchi, J. Phys. (Paris) Colloq. **38**, C7-357 (1977).
[36]K. Gschwend, H. Sato, and R. Kikuchi, J. Chem. Phys. **69**, 5006 (1978).
[37]B. Fultz and J. W. Morris, Jr., Phys. Rev. B **34**, 4480 (1986).
[38]B. Fultz, H. H. Hamdeh, and J. Okamoto, Hyperfine Interact. **54**, 799 (1990).
[39]H. H. Hamdeh, J. Okamoto, and B. Fultz, Phys. Rev. B **42**, 6694 (1990).
[40]A. G. Khachaturyan, Kristallografiya **5**, 354 (1960) [Sov. Phys. Crystallogr. **5**, 335 (1960)].